

OPEN

Improving the sustainability of biodiesel by using imidazolium-based ionic liquid

M. A. Deyab¹✉ & O. Mohsen²

Corrosion of biodiesel-filled fuel tanks has become a major problem in the use of biodiesel as a new green energy source. The ionic liquid 1-Hexyl-3-methylimidazolium bis(trifluoromethanesulfonyl) imide $[C_{10}H_{19}N_2]^+[C_2F_6NO_4S_2]^-$ was used to control corrosion of C-steel in non-edible biodiesel to resolve this problem. The anti-corrosion and antioxidant properties of the $[C_{10}H_{19}N_2]^+[C_2F_6NO_4S_2]^-$ were characterized using weight loss, electrochemical impedance spectroscopy, total acid number measurements beside SEM and EDX analysis. The findings show that $[C_{10}H_{19}N_2]^+[C_2F_6NO_4S_2]^-$ plays an important role in preventing C-steel corrosion in biodiesel with an efficiency close to 99 percent. The adsorption capability and antioxidant properties of $[C_{10}H_{19}N_2]^+[C_2F_6NO_4S_2]^-$ are the major contributors to the ionic liquid's anti-corrosion properties. We anticipate that this work will help to sustainably expand the use of biodiesel as a renewable energy source.

Biodiesel is one of the most promising renewable energy sources of the future^{1,2}. It can be used in the current diesel car engines without needing any changes to be made to them³. Principally, biodiesel is synthesized by trans-esterification process of vegetable oil with alcohol in the presence of catalyst⁴. The advantage of biodiesel over fossil fuels is that it is a clean fuel and does not cause pollution to the environment. In addition, it can be produced from non-exhaustible natural sources⁵. One of the most important obstacles that limit the widespread use of biodiesel is that it causes corrosion of fuel tanks^{6,7}.

Several previous studies have shown that the rate of corrosion in the fuel tank containing biodiesel is much higher than that containing petrodiesel.

This is due to many factors such as hygroscopic nature of biodiesel and biodiesel oxidation⁸. This leads to the presence of water and free fatty acids in the fuel tank and consequently the corrosion in the wall of tank^{9,10}. There are two methods that could be used to prevent the corrosion problem caused by the biodiesel namely: (i) use of high corrosion resistance alloys in the manufacture of fuel tank, and (ii) use of corrosion inhibitors to protect the fuel tank. High corrosion resistance alloys are expensive and require special manufacturing capabilities when used in the manufacture of fuel tanks^{11,12}. In this regard, some organic compounds, surfactants and plant extracts were used to protect the fuel tank from corrosion in biodiesel. Cardanol¹³, rosemary leaves¹⁴, span 80¹⁵, and butylated hydroxyl toluene¹⁶ were found to protect the biodiesel fuel tank from corrosion in previous our studies. In this paper, we continue our research in this area by using a new class of compounds, ionic liquids, as a new additive in non-edible Neem oil biodiesel to prevent corrosion in the fuel tank.

Ionic liquids as corrosion inhibitors should be recommended over conventional volatile and toxic corrosion inhibitors¹⁷⁻¹⁹ because of their numerous advantages, including low volatility, chemical and electrochemical stability, and the possibility of being more environmentally friendly. Furthermore, ionic liquids are frequently used in smaller quantities than conventional corrosion inhibitors, leading to reduced cost.

For the first time, the effect of 1-hexyl-3-methylimidazolium bis(trifluoromethanesulfonyl)imide $[C_{10}H_{19}N_2]^+[C_2F_6NO_4S_2]^-$ on the corrosion behavior of C-steel in biodiesel was investigated. The corrosion mechanism is also explained through adsorption isotherm and thermodynamic studies.

Materials and methods

Materials. The C-steel (composition wt%: 0.2 carbon, 0.6 manganese, 0.1 Silicon, balance Fe) substrate was purchased from Egyptian iron co. ASTM G1—03(2017)e1 standard method was used to produce clean C-steel electrode surface^{20,21}.

The ionic liquid $[C_{10}H_{19}N_2]^+[C_2F_6NO_4S_2]^-$ was purchased from Sigma-Aldrich Chemie GmbH.

¹Egyptian Petroleum Research Institute (EPRI), Nasr City, Cairo, Egypt. ²Department of Chemistry, College of Sciences, Taif University, Taif, Saudi Arabia. ✉email: hamadadeiab@yahoo.com

Property	Unit	Biodiesel	ASTM Standard Biodiesel D 6751
Appearance	–	light Yellow	Light yellow
Odor	–	Mild	Mild
Physical State	–	Liquid	Liquid
Boiling point	°C	285	338 max
Kinematic Viscosity at 40 °C	mm ² s ⁻¹	5.07	1.9–6.0
Specific gravity at 25 °C	–	0.84	0.88
Flash point	°C	157	100–170
Pour point	°C	2.1	– 15 to 10
Water content	% vol	0.03	0.05 max
Free glycerin	wt%	0.018	0.02

Table 1. Specification of synthesized biodiesel from Neem oil.

[C ₁₀ H ₁₉ N ₂] ⁺ [C ₂ F ₆ NO ₄ S ₂] ⁻ (mg/l)	v (mg cm ⁻² h ⁻¹) × 10 ⁻⁴	η _w %
Blank (Biodiesel)	2.762 ± 0.135	–
20	1.692 ± 0.124	38.7
40	0.704 ± 0.035	74.5
60	0.235 ± 0.022	91.4
80	0.030 ± 0.002	98.9
100	0.033 ± 0.002	98.8
120	0.030 ± 0.002	98.9
140	0.049 ± 0.001	98.2

Table 2. Weight loss parameters for the corrosion of C-steel in biodiesel and biodiesel containing [C₁₀H₁₉N₂]⁺[C₂F₆NO₄S₂]⁻ at 298 K.

Non-edible Neem oil was obtained from a local plant company with the following fatty acid profile: Palmitic acid (C16:0) (28.42%), Stearic acid (C18:0) (19.22%), Oleic acid (C18:1) (31.66%), Linoleic acid (C18:2) (19.40%), Arachidic acid (C20:0) (1.3%).

The synthesis of biodiesel was conducted in a conical flask containing 50 ml Neem oil, 200 ml methanol (Sigma-Aldrich) and 1.0 wt% KOH (Alfa Aesar). The experimental conditions were set at temperature of 333 K, experimental time of 3 h and stirring speed of 350 rpm. Finally, the resulting solution was allowed to settle for 24 h in order to separate the pure biodiesel and followed by washing with distilled water for several times. Water content in biodiesel was determined by coulometric Karl Fischer Titration (METTLER TOLEDO). Free and total glycerin in biodiesel was determined by gas chromatography (GC-2014, Shimadzu Corporation, Japan). Table 1 showed the physicochemical properties of the synthesized biodiesel^{22,23}. The presence of water in the biodiesel was due to the synthesis process, which included washing the transesterification product.

Methods. The weight loss WL was calculated by weighing before and after the immersion of the electrode in biodiesel for 1440 h using METTLER analytical balance. All the steps of WL were conducted according to ASTM G31-72(2004)²⁴. The initial mass and area of the substrate were 7.4763 g and 5.734 cm², respectively. The volume of biodiesel used was 100 ml. Three independent repeated experiments at the same conditions were carried out to ensure results validity. The resulted data were presented by the means and the standard deviation.

The EIS experiments were conducted in the standard cell (three electrodes: C-steel, saturated calomel electrode (SCE) reference electrode, Pt counter electrode) connected with electrochemical work-station (Gamry-3000)²⁵. EIS curves were recorded in the frequency range of 30 kHz–1.0 Hz at open circuit potential using 20 mV amplitude.

The antioxidant test and TAN calculation for biodiesel at different conditions were carried out according to ASTM D943–20 and ASTM D664–18e2, respectively^{26,27}.

The surface morphology (SEM and EDX) were conducted for C-steel samples in pure biodiesel and biodiesel containing 80 mg/l of [C₁₀H₁₉N₂]⁺[C₂F₆NO₄S₂]⁻ by Scanning Electron Microscope SEM fitted with EDX analyzer (model: ZEISS/EVO, Carl Zeiss Microscopy).

Results and discussion

Anti-corrosion properties of [C₁₀H₁₉N₂]⁺[C₂F₆NO₄S₂]⁻. To recognize the anti-corrosion properties of [C₁₀H₁₉N₂]⁺[C₂F₆NO₄S₂]⁻, the WL and EIS methods were used for C-steel in biodiesel. The effect of [C₁₀H₁₉N₂]⁺[C₂F₆NO₄S₂]⁻ on the rate of corrosion (v) and anti-corrosion performance (η_w%) of C-steel in biodiesel using the WL experiments is shown in Table 2.

Compounds	Conc mg/l	Electrode	Solution	Efficiency %	Ref
N,N'-di-sec-butyl-p-phenylenediamine	500	Copper	Biodiesel obtained from babassu oil	87	31
Ethylenediamine	100	Carbon steel	Palm biodiesel	71.8	32
Vitex negundo leaf extract	2000	Aluminium	Biodiesel (B100) produced from waste cooking oil	83	33
Tert-butylamine	100	Cast iron	Biodiesel (B100)	49.41	34
Propyl gallate	400	Carbon steel	Biodiesel (B100)	83	35
$[\text{C}_{10}\text{H}_{19}\text{N}_2]^+[\text{C}_2\text{F}_6\text{NO}_4\text{S}_2]^-$	80	Carbon steel	Biodiesel from Neem oil	98.9	This work

Table 3. Inhibition efficacy of $[\text{C}_{10}\text{H}_{19}\text{N}_2]^+[\text{C}_2\text{F}_6\text{NO}_4\text{S}_2]^-$ in biodiesel medium compared to other inhibitors described in the literature.

The v and $\eta_w\%$ were obtained using Eqs. (1) and (2)²⁸:

$$v = \frac{W}{St} \quad (1)$$

$$\eta_w\% = \frac{v_0 - v}{v_0} \times 100 \quad (2)$$

W = C-steel weight loss, S = surface area, t = time of experiment, v_0 = corrosion rate in the blank solution.

$[\text{C}_{10}\text{H}_{19}\text{N}_2]^+[\text{C}_2\text{F}_6\text{NO}_4\text{S}_2]^-$ inhibitor elicited a decrease in v at 20 mg/l (from 2.762×10^{-4} to 1.692×10^{-4} mg cm⁻² h⁻¹), and this effect was sustained until the highest inhibitor concentration (i.e. 0.049×10^{-4} mg cm⁻² h⁻¹ at 120 mg/l) (see Table 2). Inhibition of corrosion activity of C-steel in biodiesel by $[\text{C}_{10}\text{H}_{19}\text{N}_2]^+[\text{C}_2\text{F}_6\text{NO}_4\text{S}_2]^-$ was observed, with $\eta_w\%$ values ranging from 38.7% to 98.9%. We noted that $[\text{C}_{10}\text{H}_{19}\text{N}_2]^+[\text{C}_2\text{F}_6\text{NO}_4\text{S}_2]^-$ displayed the highest inhibition of 98.9% at 80 mg/l. Beyond concentration 80 mg/l, no significant change in the $\eta_w\%$ values was observed. It appears that when 80 mg/l of ionic liquid was added, the ionic liquid molecules covered nearly all of the active centers on the C-steel, and that further addition had a limited impact on the inhibition efficiency. Similar observations were noted by Cao et al.²⁹ and Arellanes-Lozada, et al.³⁰

The inhibition efficacy of $[\text{C}_{10}\text{H}_{19}\text{N}_2]^+[\text{C}_2\text{F}_6\text{NO}_4\text{S}_2]^-$ in biodiesel medium compared to other inhibitors described in the literature (see Table 3)^{31–35}.

Further inspections on the performance of $[\text{C}_{10}\text{H}_{19}\text{N}_2]^+[\text{C}_2\text{F}_6\text{NO}_4\text{S}_2]^-$ were conducted by using EIS measurements for C-steel in biodiesel without and with 80 mg/l of inhibitor. Typical EIS plots (a = Nyquist, b = Bode-phase angle, c = Bode-module, d = equivalent circuit) are shown in Fig. 1. The Nyquist plots (Fig. 1a) show one slightly depressed semicircle. Such non-ideal in the Nyquist plots is due to heterogeneity at the C-steel surface^{36–38}. Two plateaus were visible in Fig. 1c, one at high frequency and the other at low frequency. The Nyquist plots, with and without $[\text{C}_{10}\text{H}_{19}\text{N}_2]^+[\text{C}_2\text{F}_6\text{NO}_4\text{S}_2]^-$, can be described by Randles equivalent circuit (EC) as presented in Fig. 1d. In Fig. 1d, R_s is the solution resistance, C_{dl} is the double layer capacitor and R_{ct} is charge transfer resistance³⁹. It is evident that for C-steel in biodiesel containing 80 mg/l of inhibitor, R_{ct} increased from 10.5 Mohm.cm² (blank biodiesel) to 115.3 Mohm.cm². Moreover, the addition of $[\text{C}_{10}\text{H}_{19}\text{N}_2]^+[\text{C}_2\text{F}_6\text{NO}_4\text{S}_2]^-$ in biodiesel led to the decrease in the C_{dl} value from 1.51 nF cm⁻² (blank biodiesel) to 0.13 nF cm⁻². Additionally, the width of the Bode-phase angle (Fig. 1b) increases by adding $[\text{C}_{10}\text{H}_{19}\text{N}_2]^+[\text{C}_2\text{F}_6\text{NO}_4\text{S}_2]^-$, which indicates a lower corrosion rate^{40,41}. This means that $[\text{C}_{10}\text{H}_{19}\text{N}_2]^+[\text{C}_2\text{F}_6\text{NO}_4\text{S}_2]^-$ is able to impede the corrosion of C-steel in biodiesel by forming a protective layer on the C-steel surface^{42,43}.

Thermodynamic activation and adsorption isotherms studies. To estimate the performance of $[\text{C}_{10}\text{H}_{19}\text{N}_2]^+[\text{C}_2\text{F}_6\text{NO}_4\text{S}_2]^-$ at high temperatures circumstances, the v and $\eta_w\%$ values for C-steel in biodiesel without and with 80 mg/l of inhibitor were calculated in the range 298–328 K. It was noted that, under an elevated temperature of 298 K to 328 K, the $\eta_w\%$ value slightly decreases from 98.9 to 91.9% and the corrosion rate increases from $(0.030 \pm 0.002) \times 10^{-4}$ to $(0.396 \pm 0.010) \times 10^{-4}$ mg cm⁻² h⁻¹⁴⁴ (see Fig. 2). This indicates that $[\text{C}_{10}\text{H}_{19}\text{N}_2]^+[\text{C}_2\text{F}_6\text{NO}_4\text{S}_2]^-$ retains its performance at high temperature, confirming its thermal stability⁴⁵.

To assess the activation energy (E_a) for C-steel in biodiesel without and with 80 mg/l of $[\text{C}_{10}\text{H}_{19}\text{N}_2]^+[\text{C}_2\text{F}_6\text{NO}_4\text{S}_2]^-$, the variation of $\log(v)$ with $(1/T)$ was plotted, as displayed in Fig. 2, according to Arrhenius formula (Eq. 3)^{46,47}.

$$v = \lambda e^{-\frac{E_a}{RT}} \quad (3)$$

The E_a for C-steel in blank biodiesel was 4.17 kJ mol⁻¹. Whereas, with the addition of the 80 mg/l of $[\text{C}_{10}\text{H}_{19}\text{N}_2]^+[\text{C}_2\text{F}_6\text{NO}_4\text{S}_2]^-$, the value increased to 38.08 kJ mol⁻¹. This refers to the strong physical adsorption of $[\text{C}_{10}\text{H}_{19}\text{N}_2]^+[\text{C}_2\text{F}_6\text{NO}_4\text{S}_2]^-$ on the C-steel surface^{48,49}. Where the ionic liquid molecules create a large energy barrier against the corrosion process of C-steel in biodiesel⁵⁰.

The adsorption isotherm models that describe the adsorption of $[\text{C}_{10}\text{H}_{19}\text{N}_2]^+[\text{C}_2\text{F}_6\text{NO}_4\text{S}_2]^-$ on the C-steel surface based on the WL measurements were inspected.

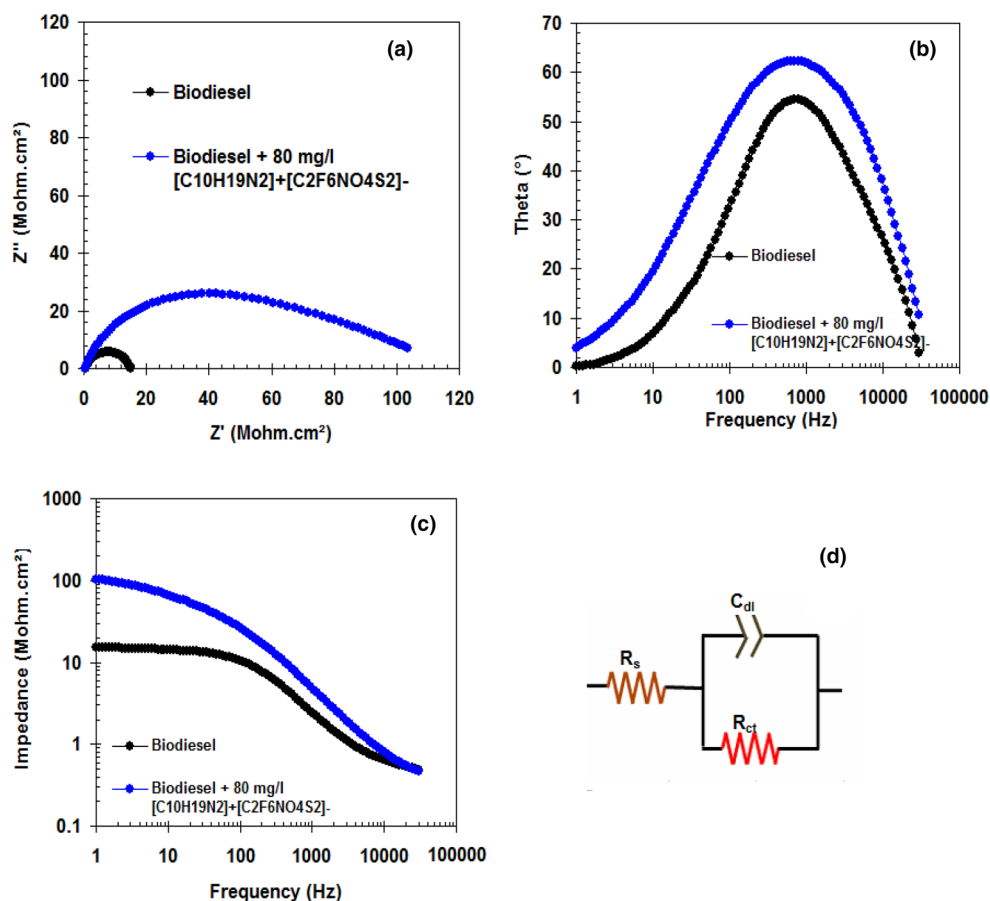


Figure 1. Typical EIS plots (a=Nyquist, b=Bode-phase angle, c=Bode-module, d= equivalent circuit) for the corrosion of C-steel in biodiesel and biodiesel containing 80 mg/l of $[C_{10}H_{19}N_2]^+[C_2F_6NO_4S_2]^-$ at 298 K.

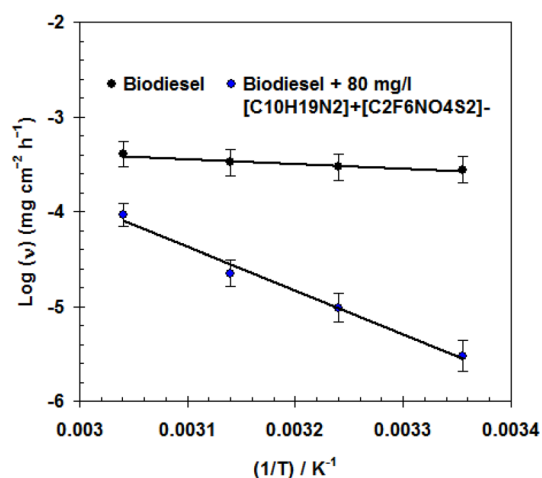


Figure 2. Arrhenius plot for C-steel in biodiesel without and with 80 mg/l of $C_{10}H_{19}N_2]^+[C_2F_6NO_4S_2]^-$.

To choose the best isotherm for the current case, various adsorption isotherm models such as Langmuir, Freundlich, and Temkin were tested (Eqs. 4, 5 and 6).

$$\frac{C_{inh}}{\theta} = \frac{1}{K_{ads}} + C_{inh} \quad \text{Langmuir} \quad (4)$$

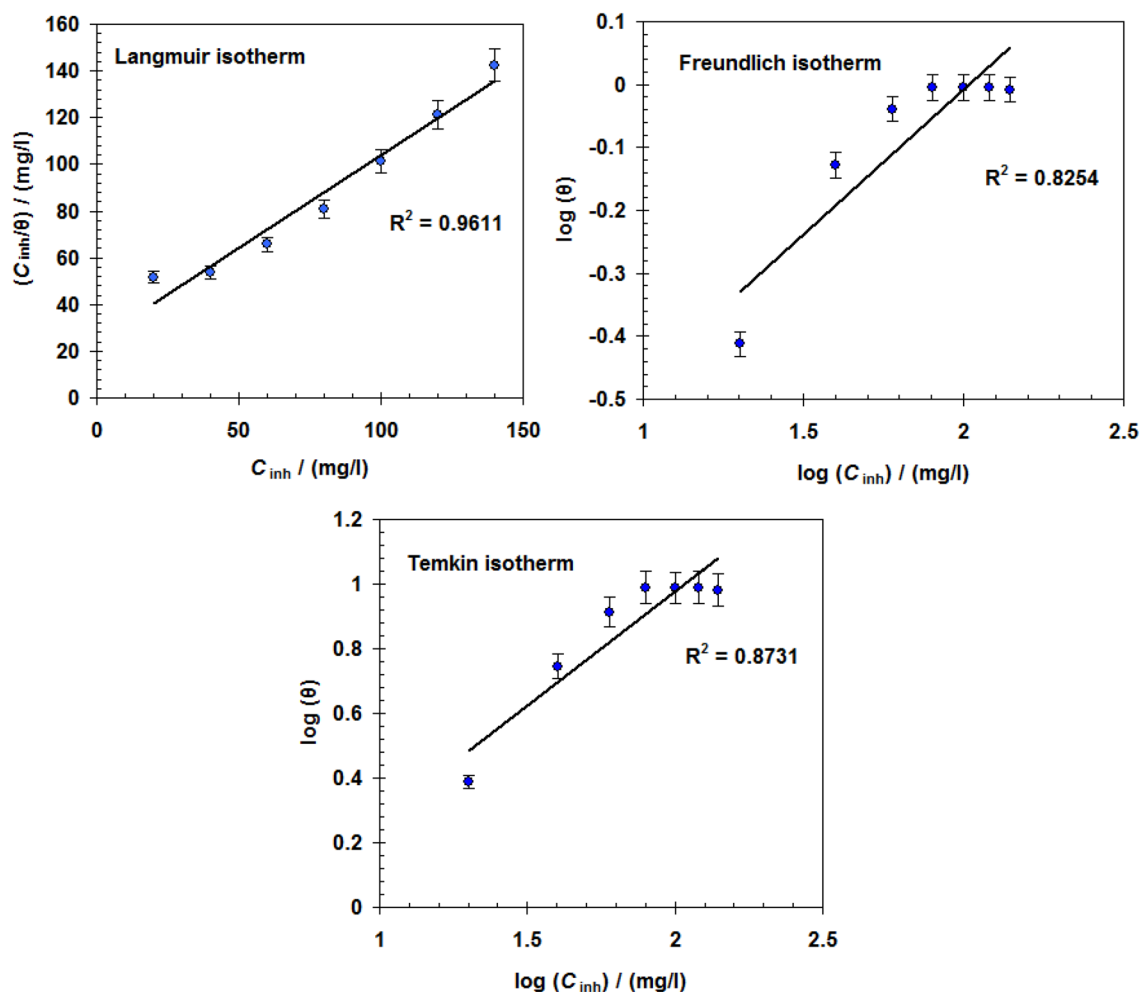


Figure 3. Various adsorption isotherm plots for $[\text{C}_{10}\text{H}_{19}\text{N}_2]^+[\text{C}_2\text{F}_6\text{NO}_4\text{S}_2]^-$ adsorption on C-steel surface in biodiesel at 298 K.

$$\theta = K_{\text{ads}}(C_{\text{inh}})^{1/n} \quad \text{Freundlich} \quad (5)$$

$$\exp(-2a\theta) = K_{\text{ads}}C_{\text{inh}} \quad \text{Temkin} \quad (6)$$

where C_{inh} is the ionic liquid concentration, K_{ads} is the equilibrium constant, “a” is the molecules interaction parameter, and θ is the surface coverage = η_w % / 100.

According to the data in Fig. 3, the Langmuir adsorption isotherm is the best isotherm for this case. This is dependent on the correlation coefficient (R^2) being close to unity⁵¹.

The K_{ads} value for the $[\text{C}_{10}\text{H}_{19}\text{N}_2]^+[\text{C}_2\text{F}_6\text{NO}_4\text{S}_2]^-$ is about $1.80 \times 10^4 \text{ M}^{-1}$.

Moreover, the Eq. 7 can be utilized to calculate the standard free energy of the adsorption reaction ($\Delta G_{\text{ads}}^\circ$)⁵².

$$\Delta G_{\text{ads}}^\circ = -RT \ln(55.5K_{\text{ads}}) \quad (7)$$

The $\Delta G_{\text{ads}}^\circ$ for the $[\text{C}_{10}\text{H}_{19}\text{N}_2]^+[\text{C}_2\text{F}_6\text{NO}_4\text{S}_2]^-$ is about $-34.16 \text{ kJ mol}^{-1}$. The negative value of $\Delta G_{\text{ads}}^\circ$ clarified the spontaneous adsorption of $[\text{C}_{10}\text{H}_{19}\text{N}_2]^+[\text{C}_2\text{F}_6\text{NO}_4\text{S}_2]^-$ molecules on the C-steel surface⁵³. Because the value of $\Delta G_{\text{ads}}^\circ$ is less than -40 kJ mol^{-1} , the type of adsorption may be physisorption or mixed type (physisorption and chemisorption)⁵⁴.

SEM and EDX analysis. The SEM and EDX analysis of C-steel in biodiesel without and with 80 mg/l of $[\text{C}_{10}\text{H}_{19}\text{N}_2]^+[\text{C}_2\text{F}_6\text{NO}_4\text{S}_2]^-$ are shown in Figs. 4 and 5. The C-steel surface, immersed in biodiesel for 1440 h, without $[\text{C}_{10}\text{H}_{19}\text{N}_2]^+[\text{C}_2\text{F}_6\text{NO}_4\text{S}_2]^-$ was extremely damaged due to the aggressive medium (Fig. 4a). EDX analysis for this case (Fig. 4b), reveals the signals for C-steel composition (i.e. C, Si, Mn, Fe) and corrosion products (i.e. iron oxide).

The impact of adding 80 mg/l of $[\text{C}_{10}\text{H}_{19}\text{N}_2]^+[\text{C}_2\text{F}_6\text{NO}_4\text{S}_2]^-$ to the biodiesel on the C-steel surface is shown in Fig. 5a. It is clear that the surface of C-steel is smooth and no corrosion products were observed on the metal

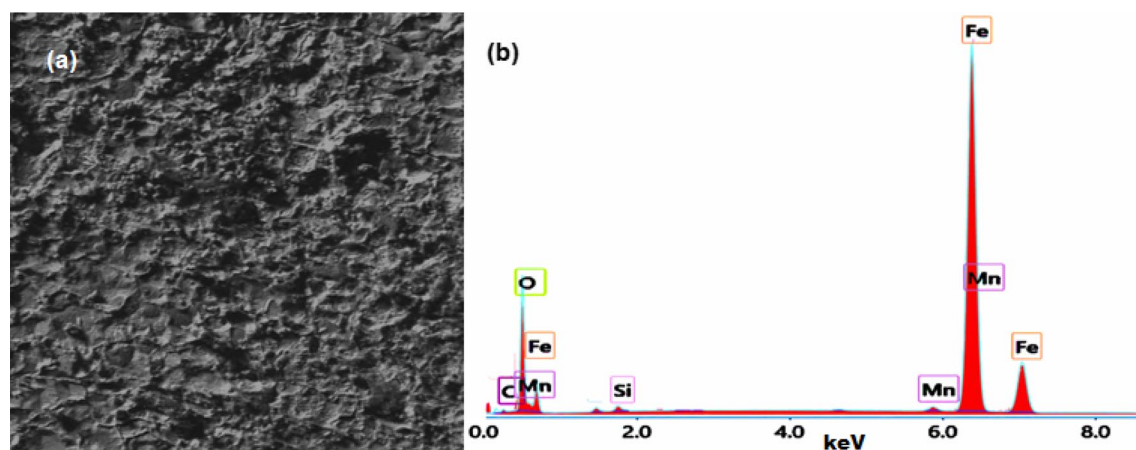


Figure 4. SEM image (a) and EDX analysis (b) of C-steel in biodiesel.

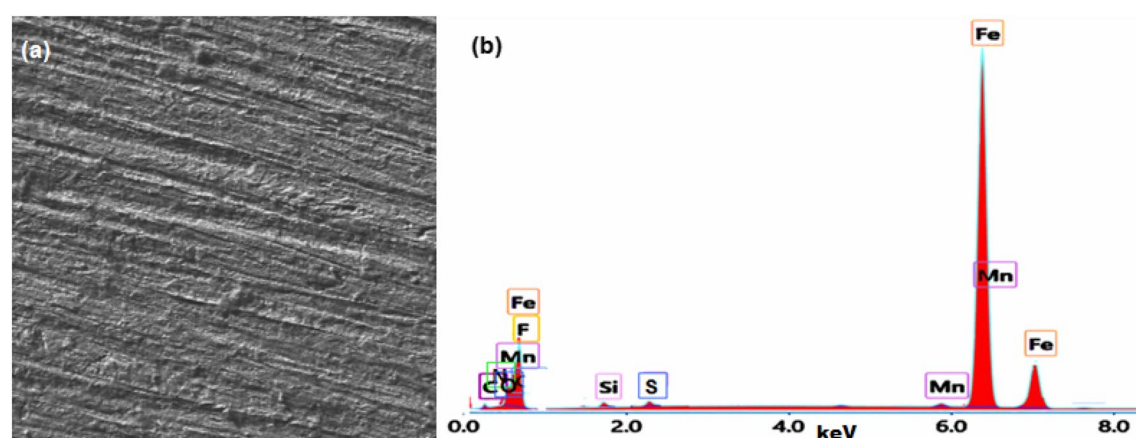


Figure 5. SEM image (a) and EDX analysis (b) of C-steel in biodiesel containing 80 mg/l of $[\text{C}_{10}\text{H}_{19}\text{N}_2]^+[\text{C}_2\text{F}_6\text{NO}_4\text{S}_2]^-$.

surface. EDX analysis for this case (Fig. 5b), reveals the signals for C-steel composition (i.e. C, Si, Mn, Fe) and characterized signals of $[\text{C}_{10}\text{H}_{19}\text{N}_2]^+[\text{C}_2\text{F}_6\text{NO}_4\text{S}_2]^-$ (i.e. C, N, F, O, S).

Mechanism of corrosion mitigation. Corrosion mitigation of C-steel in biodiesel using ionic liquid $[\text{C}_{10}\text{H}_{19}\text{N}_2]^+[\text{C}_2\text{F}_6\text{NO}_4\text{S}_2]^-$ is related to two factors. The first is the adsorption ability of $[\text{C}_{10}\text{H}_{19}\text{N}_2]^+[\text{C}_2\text{F}_6\text{NO}_4\text{S}_2]^-$ molecules on the C-steel surface to form a shielding layer^{55,56}. This layer can isolate the C-steel surface from the biodiesel⁵⁷. The presence of hetero-atoms (O, S, and N atoms) in the ionic liquid molecule affects the efficiency of this inhibitor. These atoms are commonly regarded as the reaction centre for initiating the adsorption process^{58–60}. The nonbonding electrons present on hetero-atoms, as well as π -electrons, will be transferred into the d-orbitals of the Fe atoms on the steel surface, leading to the formation of coordinate bonds between C-steel and the adsorbed ionic liquid, as observed for many organic inhibitors^{61,62}. SEM and EDX analysis verified the ionic liquid's adsorption on the C-steel surface, as shown in Figs. 4 and 5.

The second factor is the antioxidant properties of ionic liquid⁶³. This leads to the decrease in the oxidation of biodiesel and consequently, prevents the formation corrosion compounds such as free acids and aldehydes¹⁶. To confirm antioxidant properties of $[\text{C}_{10}\text{H}_{19}\text{N}_2]^+[\text{C}_2\text{F}_6\text{NO}_4\text{S}_2]^-$, the impact of adding different concentrations of $[\text{C}_{10}\text{H}_{19}\text{N}_2]^+[\text{C}_2\text{F}_6\text{NO}_4\text{S}_2]^-$ on the TAN of biodiesel was recorded and shown in Fig. 6. Inspection of Fig. 6 confirms that the presence of $[\text{C}_{10}\text{H}_{19}\text{N}_2]^+[\text{C}_2\text{F}_6\text{NO}_4\text{S}_2]^-$ leads to low TAN of biodiesel. This decreases the corrosive action of biodiesel especially during the long time storage.

Conclusions

The necessity to control corrosion in fuel tanks containing biodiesel motivated us to explore the anti-corrosion properties of ionic liquid $[\text{C}_{10}\text{H}_{19}\text{N}_2]^+[\text{C}_2\text{F}_6\text{NO}_4\text{S}_2]^-$, that could serve as informative to control the corrosion of C-steel in biodiesel. $[\text{C}_{10}\text{H}_{19}\text{N}_2]^+[\text{C}_2\text{F}_6\text{NO}_4\text{S}_2]^-$, reveals an effective new C-steel corrosion inhibitor in biodiesel. The inhibition mechanism is based on the ionic liquid's mixed physisorption and chemisorption. $[\text{C}_{10}\text{H}_{19}\text{N}_2]^+[\text{C}_2\text{F}_6\text{NO}_4\text{S}_2]^-$ molecules cover the surface of C-steel sheets, preventing biodiesel corrosive attack on steel sites. The inhibition effect is explained by this protective layer and the adsorption of an ionic liquid compound. It was clear that the $[\text{C}_{10}\text{H}_{19}\text{N}_2]^+[\text{C}_2\text{F}_6\text{NO}_4\text{S}_2]^-$ displayed the highest inhibition 98.9% at 80 mg/l. The

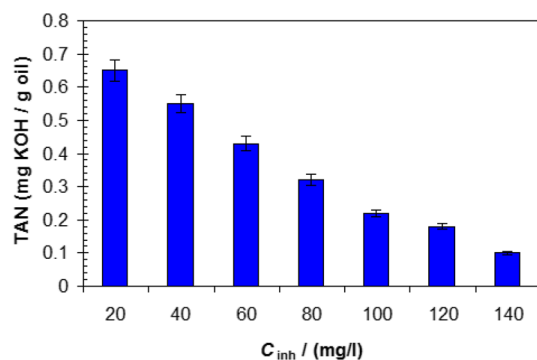


Figure 6. Variation of TAN of biodiesel with $C_{10}H_{19}N_2^+[C_2F_6NO_4S_2]^-$ concentration.

Nyquist and Bode plots conclude that the inhibition effect improves with increasing $[C_{10}H_{19}N_2^+[C_2F_6NO_4S_2]^-]$ concentration: the charge transfer resistance increases significantly while the capacitance of the electrical double layer decreases dramatically. The studies of the impact of $[C_{10}H_{19}N_2^+[C_2F_6NO_4S_2]^-]$ concentration and temperature allows for the determination of thermodynamic parameters and the confirmation of the protective role of the ionic liquid layer. The antioxidant properties of $[C_{10}H_{19}N_2^+[C_2F_6NO_4S_2]^-]$ play a significant role in explaining the anti-corrosion mechanism.

Received: 13 April 2021; Accepted: 10 August 2021

Published online: 19 August 2021

References

- Atabani, A. E. *et al.* A comprehensive review on biodiesel as an alternative energy resource and its characteristics. *Renew. Sustain. Energy Rev.* **16**(4), 2070–2093 (2012).
- Wu, X. & Leung, D. Y. Optimization of biodiesel production from camelina oil using orthogonal experiment. *Appl. Energy* **88**(11), 3615–3624 (2011).
- Mathimani, T., Senthil Kumar, T., Chandrasekar, M., Uma, L. & Prabakaran, D. Assessment of fuel properties, engine performance and emission characteristics of outdoor grown marine *Chlorella vulgaris* BDUG 91771 biodiesel. *Renew. Energy* **105**, 637–646 (2017).
- Anto, S., Pugazhendhi, A. & Mathimani, T. Lipid enhancement through nutrient starvation in *Chlorella* sp. and its fatty acid profiling for appropriate bioenergy feedstock. *Biocatal. Agric. Biotechnol.* **20**, 101179 (2019).
- Bart, J. C. J., Palmeri, N. & Cavallaro, S. Feedstocks for biodiesel production. In *Biodiesel Science and Technology* (eds Bart, J. C. J. *et al.*) 130–225 (Woodhead Publishing, 2010).
- T. Tsuchiya, H. Shiotani, S. Goto, G. Sugiyama, A. Maeda, Japanese Standards for Diesel Fuel Containing 5% FAME blended diesel fuels and its Impact on Corrosion, SAE Technical Paper No. 2006-01-3303.
- Kaul, S. *et al.* Corrosion behavior of biodiesel from seed oils of Indian origin on diesel engine parts. *Fuel Process. Technol.* **88**, 303–307 (2007).
- Dinkov, R., Hristov, G., Stratiev, D. & Aldayri, V. B. Effect of commercially available antioxidants over biodiesel/diesel blends stability. *Fuel* **88**(732), 737 (2009).
- Yamane, K., Kawasaki, K., Sone, K., Hara, T. & Prakoso, T. Oxidation stability of biodiesel and its effects on diesel combustion and emission characteristics. *Int. J. Engine Res.* **8**, 307–309 (2007).
- Wang, W., Jenkins, P. E. & Ren, Z. Heterogeneous corrosion behaviour of carbon steel in water contaminated biodiesel. *Corros. Sci.* **53**, 845–849 (2011).
- Rajasekar, A., Maruthamuthu, S., Palaniswamy, N. & Rajendran, A. Biodegradation of corrosion inhibitors and their influence on petroleum product pipeline. *Microbiol. Res.* **162**, 355–368 (2007).
- Muthukumar, N., Maruthamuthu, S. & Palaniswamy, N. Water-soluble inhibitor on microbially influenced corrosion in diesel pipeline. *Colloids and Surfaces. B, Biointerfaces* **53**, 260–270 (2006).
- Deyab, M. A., Corrêa, R. G. C., Mazzetto, S. E., Dhmees, A. S. & Mele, G. Improving the sustainability of biodiesel by controlling the corrosive effects of soybean biodiesel on aluminum alloy 5052 H32 via cardanol. *Ind. Crops Products* **130**, 146–150 (2019).
- Deyab, M. A. Corrosion inhibition of aluminum in biodiesel by ethanol extracts of Rosemary leaves. *J. Taiwan Inst. Chem. Eng.* **58**, 536–541 (2016).
- Deyab, M. A. & Keera, S. T. On corrosion and corrosion inhibition of carbon steel in stored biodiesel: electrochemical (AC and DC) studies. *J. Taiwan Inst. Chem. Eng.* **68**, 187–191 (2016).
- Deyab, M. A. The inhibition activity of butylated hydroxytoluene towards corrosion of carbon steel in biodiesel blend B20. *J. Taiwan Inst. Chem. Eng.* **60**, 369–375 (2016).
- Forsyth, M., Howlett, P. C., Somers, A. E. *et al.* Interphase engineering of reactive metal surfaces using ionic liquids and deep eutectic solvents—from corrosion control to next-generation batteries. *npj Mater. Degrad.* **1**, 18 (2017).
- Chigondo, M., Chigondo, F. Recent natural corrosion inhibitors for mild steel: an overview. *J. Chem.* **2016**, 6208937 (2016).
- Verma, C., Ebenso, E. E., Quraishi, M. A. & Hussai, C. M. Recent developments in sustainable corrosion inhibitors: design, performance and industrial scale applications. *Mater. Adv.* **2**, 3806–3850 (2021).
- ASTM G1-03(2017)e1, Standard Practice for Preparing, Cleaning, and Evaluating Corrosion Test Specimens, ASTM International, West Conshohocken, PA, 2017, www.astm.org.
- Deyab, M. A., Nada, A. A. & Hamdy, A. Comparative study on the corrosion and mechanical properties of nano-composite coatings incorporated with TiO_2 nano-particles, TiO_2 nano-tubes and ZnO nano-flowers. *Prog. Org. Coat.* **105**, 245–251 (2017).
- ASTM D6751-20a. Standard Specification for Biodiesel Fuel Blend Stock (B100) for Middle Distillate Fuels, ASTM International, West Conshohocken, PA, 2020, www.astm.org.
- Ezekoye, V., Adinde, R., Ezekoye, D. & Ofomata, A. Syntheses and characterization of biodiesel from citrus sinensis seed oil. *Sci. African* **6**, e00217 (2019).

24. ASTM G31-72(2004). Standard Practice for Laboratory Immersion Corrosion Testing of Metals, ASTM International, West Conshohocken, PA, 2004, www.astm.org.
25. Deyab, M. A. & Guibal, E. Enhancement of corrosion resistance of the cooling systems in desalination plants by green inhibitor. *Sci. Rep.* **10**, 4812 (2020).
26. ASTM D943-20. Standard Test Method for Oxidation Characteristics of Inhibited Mineral Oils, ASTM International, West Conshohocken, PA, 2020, www.astm.org.
27. ASTM D664-18e2. Standard Test Method for Acid Number of Petroleum Products by Potentiometric Titration, ASTM International, West Conshohocken, PA, 2018, www.astm.org.
28. Yu, Q., Jiang, X., Zhou, L., Xia, G. Preparation and inhibition of 2-methyl cetyl pyridine bromide for X70 steel in 5 M HCl. *Mater. Res. Innov.* **17**, 166–171 (2013).
29. Cao, S. *et al.* Green Brønsted acid ionic liquids as novel corrosion inhibitors for carbon steel in acidic medium. *Sci. Rep.* **7**, 8773 (2017).
30. Arellanes-Lozada, P., Díaz-Jiménez, V., Hernández-Cocoletzi, H., Nava, N., Olivares-Xometl, O. & Likhanova, N. V. Corrosion inhibition properties of iodide ionic liquids for API 5L X52 steel in acid medium. *Corros. Sci.* **75**, 108888 (2020).
31. Rangel, N. V. P. *et al.* Effect of additives on the oxidative stability and corrosivity of biodiesel samples derived from babassu oil and residual frying oil: an experimental and theoretical assessment. *Fuel* **289**, 119939 (2021).
32. Baena, L. M., & Calderón, J. A. (2020). Effects of palm biodiesel and blends of biodiesel with organic acids on metals. *Heliyon* **6**, e03735 (2020).
33. Subedi, B. N., Amgain, K., Joshi, S. & Bhattarai, J. Green approach to corrosion inhibition effect of Vitex negundo leaf extract on aluminum and copper metals in biodiesel and its blend. *Int. J. Corros. Scale Inhib.* **8**, 744–759 (2019).
34. Fazal, M. A., Haseeb, A. S. M. A. & Masjuki, H. H. *Fuel Process. Technol.* **92**, 2154–2159 (2011).
35. de Santana, P. M. B., Meiraa, M. & Tentardini, E. K. Effects of adding some natural substances to biodiesel to control its effect on carbon steel corrosion. *Mater. Res.* **18**, 164–169 (2015).
36. Solmaz, R., Kardaş, G., Çulha, M., Yazici, B. & Erbil, M. Investigation of adsorption and inhibitive effect of 2-mercaptothiazoline on corrosion of mild steel in hydrochloric acid media. *Electrochim. Acta* **53**, 5941–5952 (2008).
37. Kashkovskiy, R., Strelnikova, K. & Fedotova, A. Application of electrochemical impedance spectroscopy to study hydrogen sulphide corrosion of steel and its inhibition: a review. *Corros. Eng. Sci. Technol.* **54**, 493–515 (2019).
38. Guo, H. *et al.* Imidazolium ionic liquid bearing urea moiety as a new corrosion inhibitor of mild steel. *J. Mol. Liq.* **334**, 116484 (2021).
39. Deyab, M. A., El Bali, B., Essehli, R., Ouarsal, R., Lachkar, M. & Fuess, H. NaNi(H₂PO₃)₃·H₂O as a novel corrosion inhibitor for X70-steel in saline produced water. *J. Mol. Liq.* **216**, 636–640 (2016).
40. Falzone, G., Balonis, M., Bentz, D., Jones, S. & Sant, G. Anion capture and exchange by functional coatings: new routes to mitigate steel corrosion in concrete infrastructure. *Cem. Concr. Res.* **101**, 82–92 (2017).
41. Garcia, J. *et al.* Effect of cathodic protection on steel–concrete bond strength using ion migration measurements. *Cem. Concr. Compos.* **34**, 242–247 (2012).
42. Tang Fujian, C. G. & Brow, R. K. Chloride-induced corrosion mechanism and rate of enamel- and epoxy-coated deformed steel bars embedded in mortar. *Cem. Concr. Res.* **82**, 58–73 (2016).
43. Deyab, M. A. Corrosion inhibition of heat exchanger tubing material (titanium) in MSF desalination plants in acid cleaning solution using aromatic nitro compounds. *Desalination* **439**, 73–79 (2018).
44. Zeng, X., Zheng, X., Guo, L., Xu, Q., Huang, H. & Tan, B. Three imidazole ionic liquids as green and eco-friendly corrosion inhibitors for mild steel in sulfuric acid medium. *J. Mol. Liq.* **324**, 115063 (2021).
45. Deyab, M. A. 1-Allyl-3-methylimidazolium bis(trifluoromethylsulfonyl)imide as an effective organic additive in aluminum-air battery. *Electrochim. Acta* **244**, 178–183 (2017).
46. Gerengi, H. U., Solomon, I., Yildiz, M., Goksu, H. Evaluation of the inhibitive effect of Diospyros kaki (Persimmon) leaves extract on St37 steel corrosion in acid medium. *Sustain. Chem. Pharm.* **4**, 57–66 (2016).
47. Mu., G. & Li, X. Inhibition of cold rolled steel corrosion by Tween-20 in sulfuric acid: weight loss, electrochemical and AFM approaches. *J. Colloid Interface Sci.* **289**, 184–192 (2005).
48. Wadhvani, P. M., Ladha, D. G., Panchal, V. K. & Shah, N. K. Enhanced corrosion inhibitive effect of p-methoxybenzylidene-4,4-dimorpholine assembled on nickel oxide nanoparticles for mild steel in acid medium. *RSC Adv.* **5**, 7098–7111 (2015).
49. Schmid, G. M. & Huang, H. J. Spectro-electrochemical studies of the inhibition effect of 4, 7-diphenyl -1, 10-phenanthroline on the corrosion of 304 stainless steel. *Corros. Sci.* **20**, 1041–1057 (1980).
50. Qiang, Y. J., Zhang, S. T., Xu, S. Y. & Li, W. P. Experimental and theoretical studies on the corrosion inhibition of copper by two indazole derivatives in 3.0% NaCl solution. *J. Colloid Interf. Sci.* **472**, 52–59 (2016).
51. Luna, M. C., Le Manh, T., Cabrera Sierra, R., Medina Flores, J. V., Lartundo Rojas, L., Arce Estrada, E. M.. Study of corrosion behavior of API 5L X52 steel in sulfuric acid in the presence of ionic liquid 1-ethyl 3-methylimidazolium thiocyanate as corrosion inhibitor. *J. Mol. Liq.* **28** 111106 (2019)
52. Deyab, M. A. Effect of nonionic surfactant as an electrolyte additive on the performance of aluminum-air battery. *J. Power Sources* **412**, 520–526 (2019).
53. Bouklah, M., Hammouti, B., Lagrenee, M. & Bentiss, F. Thermodynamic properties of 2, 5-bis(4-methoxyphenyl)-1, 3, 4-oxadiazole as a corrosion inhibitor for mild steel in normal sulfuric acid medium. *Corros. Sci.* **48**, 2831–2842 (2006).
54. Lgaz, H. *et al.* Correlated experimental and theoretical study on inhibition behavior of novel quinoline derivatives for the corrosion of mild steel in hydrochloric acid solution. *J. Mol. Liq.* **244**(Supplement C), 154–168 (2017).
55. Li, Y., Zhang, S., Ding, Q., Qin, B. & Hu, L. Versatile 4, 6-dimethyl-2-mercaptopyrimidine based ionic liquids as high-performance corrosion inhibitors and lubricants. *J. Mol. Liq.* **284**, 577–585 (2019).
56. Likhanova, N. V. *et al.* Effect of organic anions on ionic liquids as corrosion inhibitors of steel in sulfuric acid solution. *J. Mol. Liq.* **279**, 267–278 (2019).
57. Roberge, P. R. Corrosion Engineering. Corrosion Electrochemistry, Chapter (McGraw-Hill, 2008).
58. Deyab, M. A. Efficiency of cationic surfactant as microbial corrosion inhibitor for carbon steel in oilfield saline water. *J. Mol. Liq.* **255**, 550–555 (2018).
59. El Bakri, Y., Guo, L., Anouar, E. H. & Essassi, E. M. Electrochemical, DFT and MD simulation of newly synthesized triazolotriazine derivatives as corrosion inhibitors for carbon steel in 1 M HCl. *J. Mol. Liq.* **274**, 759–769 (2019).
60. Arellanes-Lozada, P. *et al.* Adsorption and performance of ammonium-based ionic liquids as corrosion inhibitors of steel. *J. Mol. Liq.* **265**, 151–163 (2018).
61. Fuchs-Godec, R. The adsorption, CMC determination and corrosion inhibition of some N-alkyl quaternary ammonium salts on carbon steel surface in 2 M H₂SO₄. *Colloid Surf. A.* **280**, 130–139 (2006).
62. Verma, C., Ebenso, E. E., Vishal, Y. & Qurashi, M. A. Dendrimers: a new class of corrosion inhibitors for mild steel in 1M HCl: Experimental and quantum chemical studies. *J. Mol. Liq.* **224**, 1282–1293 (2016).
63. Ahmad, N. A. *et al.* Synthesis, characterisation and antioxidant properties of ferulate-based protic ionic liquids: experimental and modelling approaches. *J. Mol. Liq.* **278**, 309–319 (2019).

Acknowledgements

Taif University Researchers Supporting Project number (TURSP-2020 /19), Taif University ,Saudi Arabia.

Author contributions

M.A. Deyab: Conceptualization; Data curation; Formal analysis; Investigation; Methodology; Project administration; Resources; Software; Supervision; Validation; Visualization; Roles/Writing—original draft; Writing—review & editing. Q. Mohsen: Funding acquisition; Software; Writing—review & editing.

Competing interests

The authors declare no competing interests.

Additional information

Correspondence and requests for materials should be addressed to M.A.D.

Reprints and permissions information is available at www.nature.com/reprints.

Publisher's note Springer Nature remains neutral with regard to jurisdictional claims in published maps and institutional affiliations.



Open Access This article is licensed under a Creative Commons Attribution 4.0 International License, which permits use, sharing, adaptation, distribution and reproduction in any medium or format, as long as you give appropriate credit to the original author(s) and the source, provide a link to the Creative Commons licence, and indicate if changes were made. The images or other third party material in this article are included in the article's Creative Commons licence, unless indicated otherwise in a credit line to the material. If material is not included in the article's Creative Commons licence and your intended use is not permitted by statutory regulation or exceeds the permitted use, you will need to obtain permission directly from the copyright holder. To view a copy of this licence, visit <http://creativecommons.org/licenses/by/4.0/>.

© The Author(s) 2021